1 Electronic Supplementary Information

2 Kinetic Processes of Phase Separation and Aggregation Behaviors

3 in Slot-die Processed High Efficiency Y6-based Organic Solar Cells

4

5 Jingwei Xue, ‡[a] Hafiz Bilal Naveed, ‡ [a] Heng Zhao,[a] Baojun Lin,[a] Yilin Wang,[a] Qinglian

6 Zhu,[a] Baohua Wu,[a] Zhaozhao Bi,[a] Xiaobo Zhou,[a] Chao Zhao,[a] Ke Zhou*[a] and Wei Ma*[a]

7

8 J. Xue, H. Zhao, B. Lin, Y. Wang, Q. Zhu, B. Wu, Z. Bi, X. Zhou, Dr. C. Zhao, Dr. K.

9 Zhou, Prof. W. Ma

10 State Key Laboratory for Mechanical Behavior of Materials, Xi'an Jiaotong University,

11 Xi'an 710049, China

12 *Corresponding author. E-mail: msekzhou@xjtu.edu.cn; msewma@xjtu.edu.cn

13

14 **Experiment section**

15 **Materials**.   D18   poly[(2,6-(4,8-bis(5-(2-ethylhexyl-3-fluoro)thiophen-2-yl)-benzo[1,2-

16 b:4,5-b′]dithiophene))-alt-(2-butyloctyl)   thiophen-2-yl)-8-(4-(2-butyloctyl)-5-

17 methylthiophen-2-yl)dithieno[3′,2′:3,4;2″,3″:5,6]benzo[1,2-c][1,2,5]thiadiazole)]) and Y6

18 (2,2′-((2Z,2′Z)-((12,13-bis(2-ethylhexyl)-3,9-diundecyl-12,13-dihydro-

19 [1,2,5]thiadiazolo[3,4-e]thieno[2″,3″:4′,5′]thieno[2′,3′:4,5]pyrrolo[3,2-

20 g]thieno[2′,3′:4,5]thieno[3,2-b]indole-2,10-diyl)bis(methanylylidene)) bis(5,6-difluoro-3-

1   oxo-2,3-dihydro-1H-indene-2,1-diylidene)) dimalononitrile) were purchased from Hyper,

2   Inc. PM6 Poly[(2,6-(4,8-bis(5-(2-ethylhexyl-3-fluoro)thiophen-2-yl)-benzo[1,2-b:4,5-

3   b']dithiophene))-alt-(5,5-(1',3'-di-2-thienyl-5',7'-bis(2-ethylhexyl)benzo[1',2'-c:4',5'-

4   c']dithiophene-4,8-dione)] was purchased from Solarmer Materials Inc. All chemicals

5   were used as received without further purification. The patterned glass/ITO substrates were

6   purchased from South China Science & Technology Co., Ltd. The patterned PET/ITO

7   substrates were purchased from Youxuan New Energy Technology Co., Ltd. The ZnO

8   precursor was prepared by dissolving zinc acetate dehydrate in 2-methoxyethanol with

9   ethanolamine[1].

10

11   **Device Fabrication**.

12   The BHJ devices were fabricated with an inverted device structure of glass/ITO/ZnO/active

13   layer/MoO$_3$/Al. The patterned ITO substrate was continuously cleaned three times by

14   sonication in water with detergent, deionized water, acetone, and isopropanol for 30 min

15   of each step. Then the substrate was dried with a nitrogen gun. After ultraviolet ozone

16   treatment for 20 min, the ZnO precursor was spin-coated on the ITO substrate at 4500 rpm

17   to form an electron transporting layer ZnO. Then, the substrate was baked at 200 °C for 30

18   min. Three solvents were used in the experiments containing chloroform, chlorobenzene

19   and mixed solvents (MS) (CF as the primary solvent with 0.5% v/v CB). For D18:Y6 the

20   active layer solution was prepared in three solvents at a total concentration of 8 mg/mL

21   (D/A = 1:1.6 by weight) without any additives. For PM6:Y6 the active layer solution was

22   prepared in three solvents at a total concentration of 16 mg/mL (D/A = 1:1.2 by weight)

23   without any additives. After that, a 110 nm film of the active layer was coated by slot-die

coating in ambient conditions. For the slot-die coating, the solution was pumped onto a moving substrate through the slot in the coating head. The gap between the substrate and the head was 100 μm. The substrate temperature were controlled by heating element. The speed of the substrate and the injection speed of the solution were adjusted to obtain different active layer thickness. The final BHJ films were transferred to the N2-filled glovebox without any further treatment. Finally, a 10 nm MoO_3 and 100 nm Al were sequentially deposited as anode below the vacuum level of 1×10^{-4} Pa. The device active area of small-area device is 0.04 cm^2.

Characterization. The UV−vis absorption spectrum was measured by a Shimadzu UV-3600 Plus Spectrophotometer. The film thickness was measured by a surface profilometer (Dektak XT, Bruker). The $J-V$ characteristics were performed in a N2-filled glovebox under AM 1.5G (100 mW/cm2) using a Keithley 2400 source meter unit and an AAA solar simulator (SS-F5-3A, Enli Technology CO., Ltd.) calibrated by a standard Si photovoltaic cell with a KG5 filter. The EQE was measured by a solar cell spectral response measurement system (QE-R3018, Enli Technology CO., Ltd.) with the calibrated light intensity by a standard single-crystal Si photovoltaic cell. TEM characterization was performed by a FEI Talos F200c transmission electron microscope at 200 kV. AFM characterization was scanned by Veeco INNOVA Atomic Force Microscope using a tapping mode. The contact angle was obtained by KRUSS DSA 100 with water and diiodomethane.

Hole and Electron Mobility Measurements. The mobilities were measured by using a space charge limited current (SCLC) model with the hole-only device of

glass/ITO/PEDOT:PSS/active layer/MoO_X/Al and electron-only device of glass/ITO/ZnO/ active layer /PDINO/Al. Hole mobility and electron mobility were obtained by fitting the current density-voltage curves and calculated by the equation [2,3]:

$$J = 9\varepsilon_0\varepsilon_r\mu(V_{appl} - V_{bi} - V_s)^2/8L^3$$

Where J is current density, ε_0 is the permittivity of free space, ε_r is the relative permittivity of the material (assumed to 3), μ is hole mobility or electron mobility, V_{appl} is applied voltage, V_{bi} is the buit-in voltage due to the relative work function difference of the two elcetrodes, V_s is the voltage drop from the substrate's series resistance (V_s=IR) and L is the thickness of active layer.

Grazing Incidence Wide-Angle X-ray Scattering (GIWAXS) Characterization. GIWAXS measurements[4] were performed at beamline 7.3.3 at the Advanced Light Source. Samples were prepared on Si substrates using identical blend solutions as those used in devices. The 10 keV X-ray beam was incident at a grazing angle of 0.10-0.16°, selected to maximize the scattering intensity from the samples. The scattered x-rays were detected using a Dectris Pilatus 2 M photon counting detector.

Resonant Soft X-ray Scattering (RSoXS): RSoXS[5,6] transmission measurements were performed at beamline 11.0.1.2 at the Advanced Light Source. Samples for RSoXS measurements were prepared on a PSS modified Si substrate under the same conditions as those used for device fabrication, and then transferred by floating in water to a 1.5 mm×1.5 mm, 100 nm thick Si3N4 membrane supported by a 5 mm×5 mm, 200 μm thick Si frame (Norcada Inc.). 2D scattering patterns were collected on an in-vacuum CCD camera (Princeton Instrument PI-MTE). The sample detector distance was calibrated from diffraction peaks of a triblock copolymer poly(isoprene-b-styrene-b-2-vinyl pyridine),

1   which has a known spacing of 391 Å. The beam size at the sample is approximately 100

2   μm by 200 μm. Near the carbon absorption edge (around 285 eV, which is in the soft X-ray

3   range), the index of refraction of polymers varies drastically and uniquely, yielding

4   extremely varying and high contrast[7]. In our systems, the index of refraction of materials

5   also varies drastically and uniquely near the carbon absorption edge. We have employ the

6   R-SoXS measurements at different energy (270, 282, 283, 284.2, 284.8, 285.2, 285.8,

7   286.8 eV) near the carbon absorption edge to get the high contrast. Finally, we found the

8   scattering at 284.2 eV get the highest contrast.

9   The relative domain purity can be extracted by integrating the R-SoXS scattering profiles

10   via total scattering intensity (TSI).(Modern Aspects of Small-Angle Scattering. Kluwer

11   Academic Publishers: Dordrecht, 1995, 45, 463. Colloid Polym. Sci. 1952 , 125 , 108 .

12   Small Angle X-ray Scattering (Eds: O. Glatter , O. Kratky),Academic Press , London 1982

13   .)

$$TSI = \int_0^\infty I(q)q^2dq = 2\pi^2V\sum_{i \neq j}\Delta\rho_{ij}^2\phi_i\phi_j$$

14

15   where $\Delta\rho_{ij}$ is for the conventional SAXS the difference in electron density between the

16   i^{th} and j^{th} phases, ϕ_i is the volume fraction of ith phase and it follows that $\sum\phi_i = 1$. Note

17   that $\Delta\rho_{ij}$ becomes the difference in composition between the ith and j^{th} phases in R-SoXS

18   and $\Delta\rho_{ij}^2$ is proportional to the optical contrast of $\Delta n^2 = \Delta\delta_{ij}^2 + \Delta\beta_{ij}^2$, where $\Delta\delta_{ij}$ and $\Delta\beta_{ij}$

19   are the difference of dispersive and absorptive optical constants, respectively.

20   Subsequently it is helpful to define Δc_{ij} as a parameter describing the average composition

21   variation between the ith and j^{th} phases. The TSI expression can then be rewritten as

$$TSI = \int_0^\infty I(q)q^2 dq = 2\pi^2 V \sum_{i \neq j} \Delta c_{ij}^2$$

1

2 To be more specific, in a two-phase system the TSI can be simplified to

$$TSI = \int_0^\infty I(q)q^2 dq = 2\pi^2 V \Delta \rho_{12}^2 \phi_1 \phi_2 = 2\pi^2 V \Delta c_{12}^2$$

3

4 where $\phi_2 = 1 - \phi_1$. Given the straightforward relation between ϕ_1 and ϕ_2, the average

5 composition variation is proportional to domain purity[8].

6

7 **In-situ Ultraviolet-visible (UV-vis) Absorption Measurements**. In-situ UV-vis

8 absorption measurements were performed by the Filmetrics F20-EXR spectrometer using

9 the transmission mode with the time resolution of 0.04 s. The spectrometer consists of light

10 source and detector. The light source and detector are fixed above and below the substrate,

11 respectively, and on the same vertical line. The solution was injected into the slot and the

12 film was coated onto the glass substrate. The detector collects the transmission spectra

13 ranged from 400 to 1050 nm during coating. The UV-vis absorption spectra are calculated

14 from the transmission spectra according to the equation $A_\lambda = - \log_{10}(T)$, where A_λ is the

15 absorbance at a certain wavelength (λ) and T is the calculated transmittance. The light

16 source and detector were turned on before coating the film, so time zero is the point when

17 the first solution transmission spectrum was collected by the detector. Before time zero,

18 there is only noise in the transmission spectra.

19

1 **In-situ Photoluminescence Spectra Measurements**. In-situ Photoluminescence Spectra

2 Measurements were performed by a laser device (MGL-III-532nm-300m W-BH80018)

3 with time resolution of 0.1s. The excitation wavelength was 532 nm.

4

5

6

7 **Table S1.** The summarized surface free energy, solubility parameters, and interaction

8 parameters.

i	γ_s [mN m^{-1}]	δ [Mpa$^{1/2}$]	χ [Y6,i]
Y6	44.44	24.45	/
D18	34.11	21.42	0.64
PM6	35.15	21.75	0.58

9

10 **Table S2**. The Phase Separation Parameters of D18:Y6 and PM6:Y6 blend active layers

11 with different solvents.

active layer	solvent	q [nm^{-1}]	domain size [nm]
	CF	0.181	17.32
D18:Y6	0.5%CB	0.157	23.84
	CB	0.072	43.48
	CF	0.095	32.98
PM6:Y6	0.5%CB	0.093	33.90
	CB	0.078	40.19

12

13

1

2

3

4

5

6

7
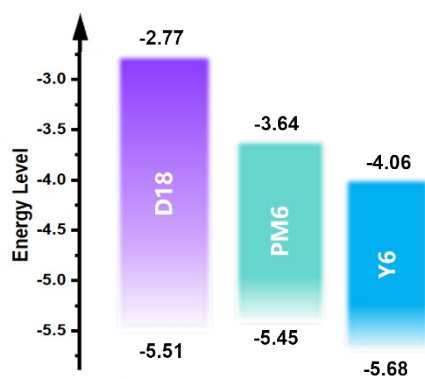
Figure S1. The energy levels of D18, PM6, and Y6.

9

10
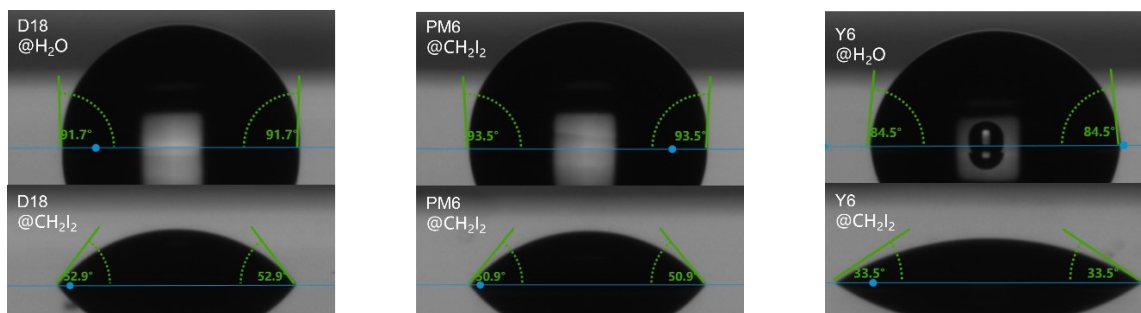
Figure S2. Contact angles of D18, PM6 and Y6.

12

13
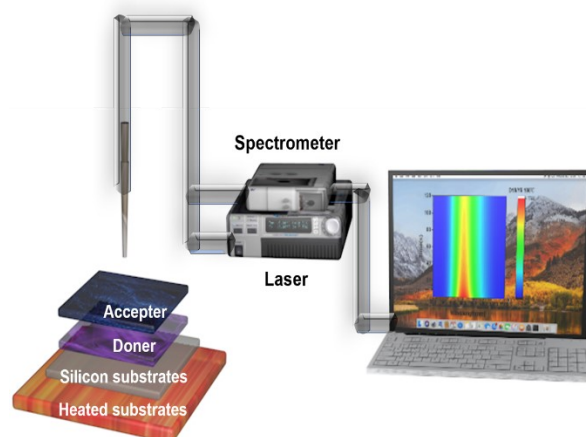
1

2 **Figure S3**. Schematic illustration of in situ PL spectra measurement of double-layer

3 structure under heating at 100°C.

4
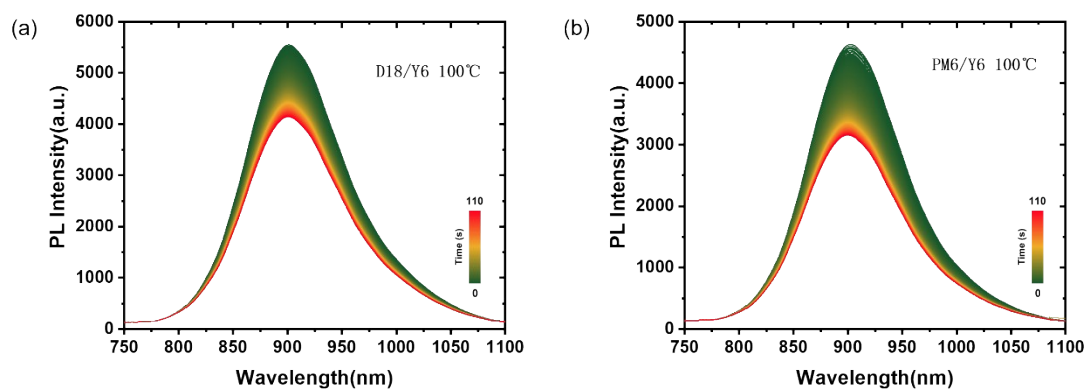
5

6 **Figure S4.** In-situ PL spectra excited at 785 nm for (a) D18/Y6 and (b) PM6/Y6 for double-

7 layer structure heated at 100 °C for 110 s.

8

9
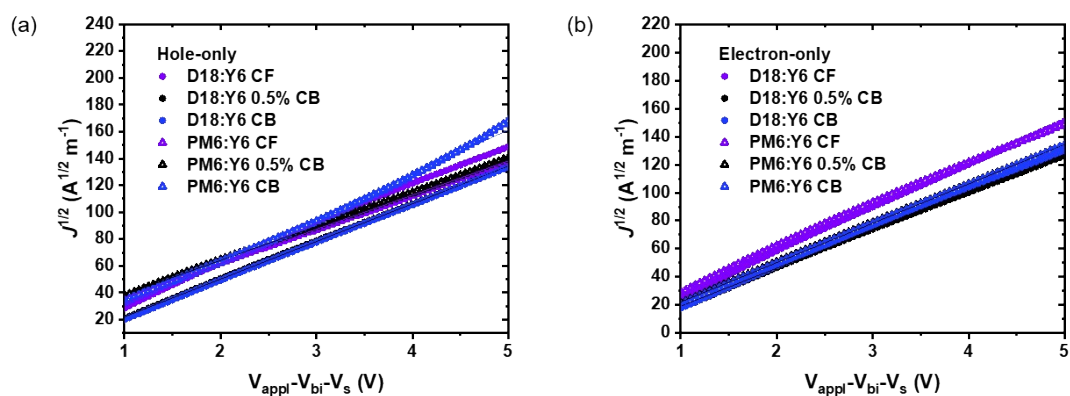
1

2 **Figure S5.** $J^{1/2}$-V characteristics of (a) hole-only and (b) electron-only devices for D18:Y6

3 and PM6:Y6 devices.
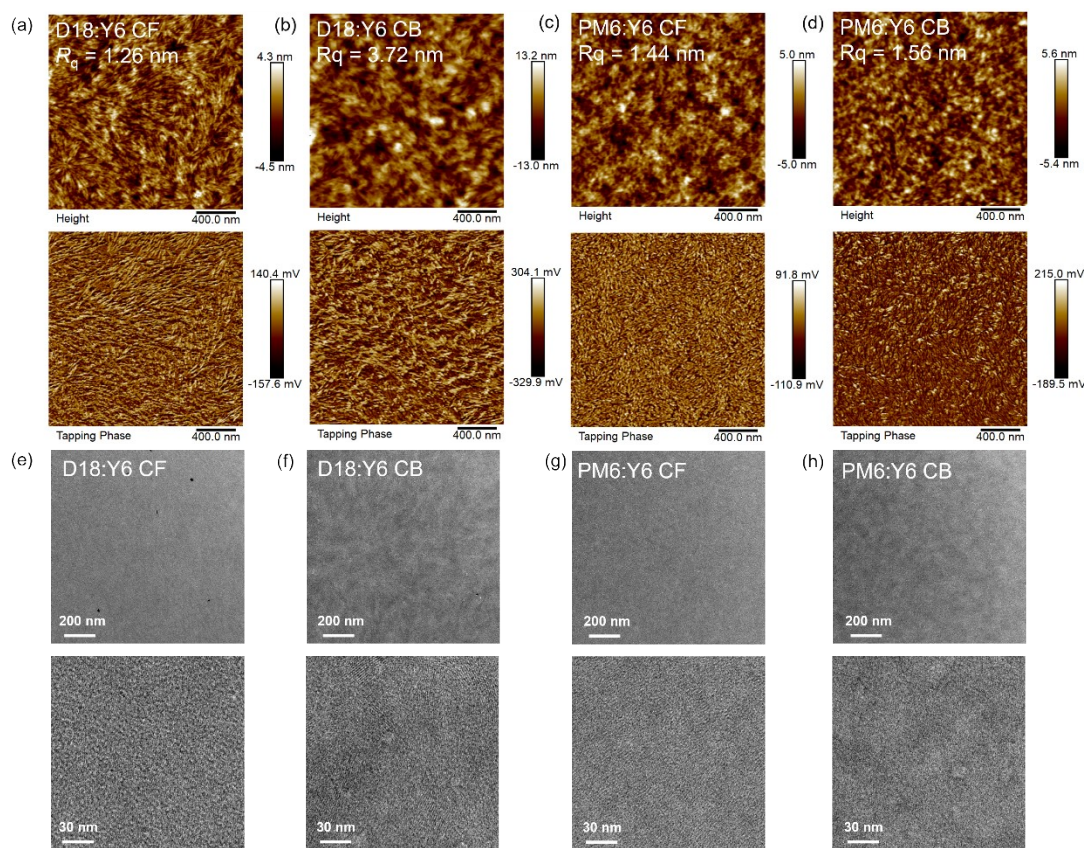
4

5 **Figure S6**. AFM height and phase images for the (a-b) D18:Y6 and (c-d) PM6:Y6 blend

6 films in different solvents. TEM images with different scales for blend films based

7 on (e-f) D18:Y6 and (g-h) PM6:Y6 in different solvents.
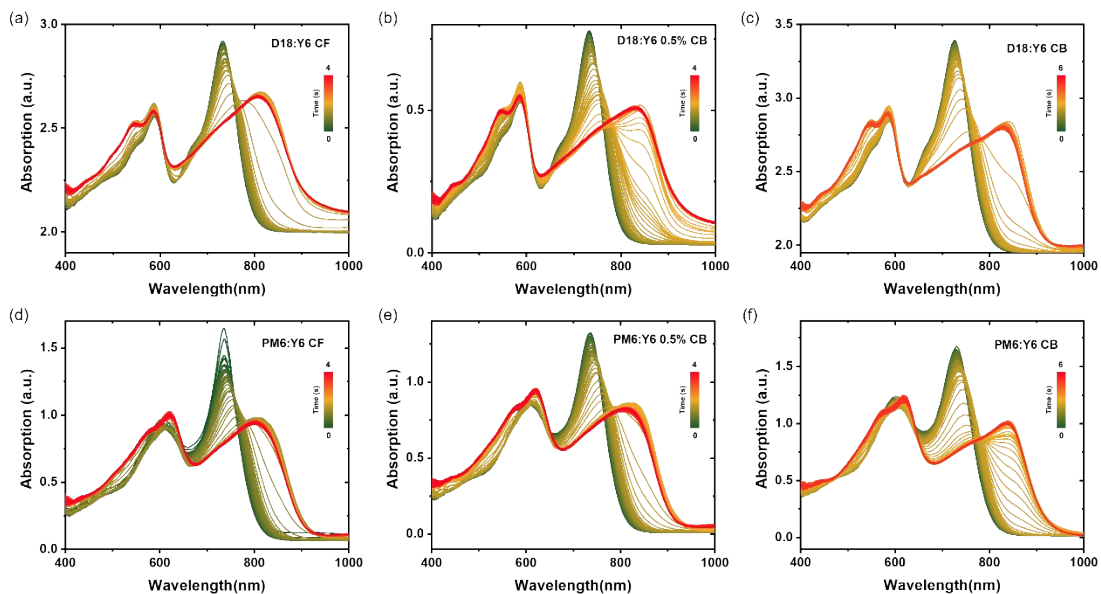
Figure S7. In-situ UV-vis absorption spectra during slot-die coating of D18:Y6 (a-c) and PM6:Y6 (d-f).
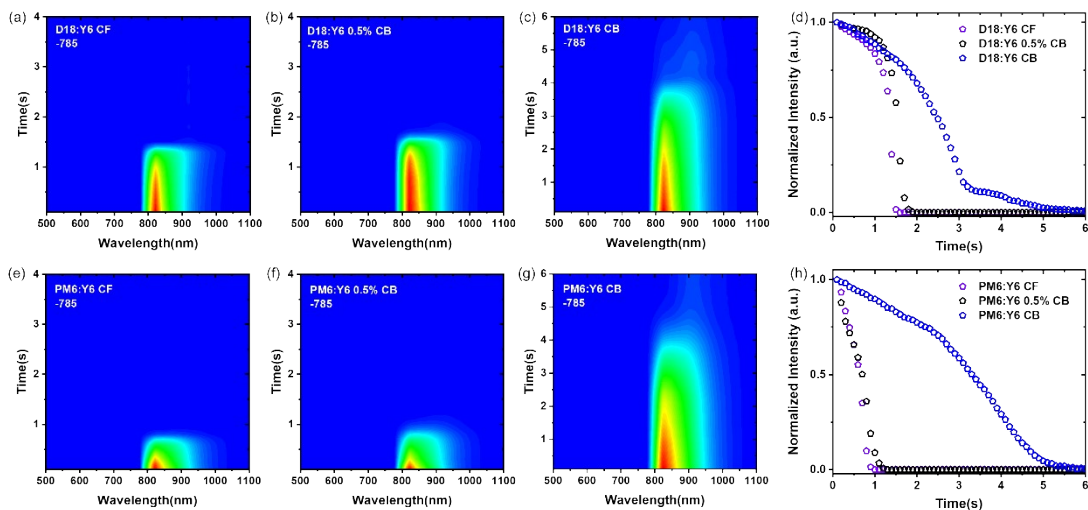
Figure S8. Time-dependent contour maps of PL spectra during slot-die coating with D18:Y6 (a-c) and PM6:Y6 (d-f) blends. Time evolution of integral PL intensity during slot-die coating with D18:Y6 (d) and PM6:Y6 (h) blends. Y6 was excited in the PL spectra at 785nm.

1
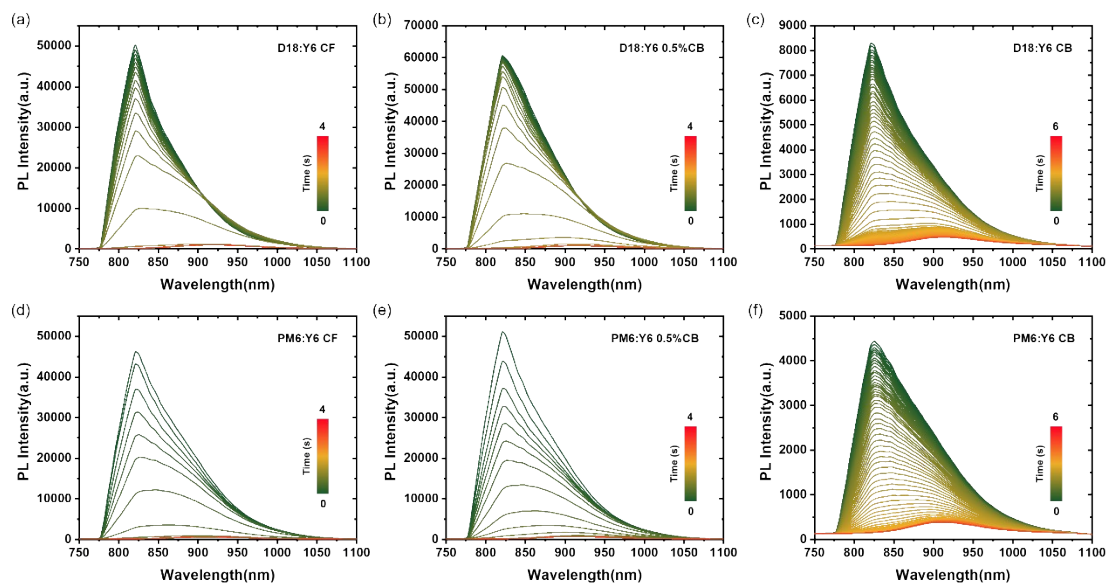
3 **Figure S9**. In-situ PL spectra during slot-die coating of D18:Y6 (a-c) and PM6:Y6 (d-f).

4

5

6

7

8

9

10

11

12

13

14

15

16

1

References

3

4 1. L. Zhan, S. Li, H. Zhang, F. Gao, T. K. Lau, X. Lu, D. Sun, P. Wang, M. Shi, C. Z. Li
5   and H. Chen, *Adv. Sci.*, 2018, **5**, 1800755.
6 2. S. Chen, Y. Liu, L. Zhang, P. C. Y. Chow, Z. Wang, G. Zhang, W. Ma and H. Yan, *J.
7   Am. Chem. Soc.*, 2017, **139**, 6298–6301.
8 3. J. A. Bartelt, D. Lam, T. M. Burke, S. M. Sweetnam and M. D. McGehee, *Adv. Energy
9   Mater.*, 2015, **5**, 1500577.
10 4. A. Hexemer, W. Bras, J. Glossinger, E. Schaible, E. Gann, R. Kirian, A. MacDowell,
11   M. Church, B. Rude and H. Padmore, *J. Phys. Conf. Ser.*, 2010, **247**, 012007.
12 5. W. Yang, W. Zaiyu, M. Xiangyi and M. Wei, *Prog. Chem.* **2017**, 29, 93.
13 6. E. Gann, A. T. Young, B. A. Collins, H. Yan, J. Nasiatka, H. A. Padmore, H. Ade, A.
14   Hexemer, C. Wang, *Rev. Sci. Instrum.* **2012**, 83, 045110.
15 7. L. Ye, S. J. Stuard and H. Ade, *Conjugated Polymers*, *CRC Press*, **2019**, 427.
16 8. X. Jiao, L. Ye and H. Ade, *Adv. Energy Mater.*, 2017, **7**, 1700084.

17

18